AIAA JOURNAL
Vol. 30, No. 6, June 1992

# Measurements in a Leading-Edge Separation Bubble due to a Simulated Airfoil Ice Accretion

M. B. Bragg* and A. Khodadoust†
*University of Illinois at Urbana-Champaign, Urbana, Illinois 61801*
and
S. A. Spring‡
*CFD Research Corporation, Huntsville, Alabama 35805*

**The separation bubble formed on an airfoil at low Reynolds number behind a simulated leading-edge glaze ice accretion is studied experimentally. Surface pressure and split hot-film measurements as well as flow visualization studies of the bubble reattachment point are reported. The simulated ice generates an adverse pressure gradient that causes a laminar separation bubble of the long bubble type to form. The boundary layer separates at a location on the ice accretion that is independent of angle of attack and reattaches at a downstream location 5–40% chord behind the leading edge, depending on the angle of attack. Velocity profiles show a large region of reverse flow that extends up from the airfoil surface as much as 2.5% chord. After reattachment, a thick distorted turbulent boundary layer exists. The separation bubble growth and reattachment are clearly seen in the plots of boundary-layer momentum thickness vs surface distance. Local minima and maxima in the boundary-layer momentum thickness development compare well with the shear layer transition point as indicated by the surface pressures and the reattachment point as measured from surface oil flow, respectively.**

## I. Introduction

ICE accretes on airfoils under certain conditions to form a large leading-edge protuberance. A laminar leading-edge separation bubble forms on the airfoil due to this modified airfoil geometry. As a result of the ice accretion and separation bubble, the airfoil suffers a large increase in drag and a significant decrease in maximum lift.[1] Understanding the behavior of the bubble is critical to an understanding of the effect of ice accretion on airfoil aerodynamics.

Laminar separation bubbles on airfoils have been widely studied. Several excellent review articles, including that by Tani,[2] summarize the fundamentals. A sketch of a laminar separation bubble, adapted from Roberts,[3] is shown in Fig. 1. The bubble forms when a laminar boundary layer encounters an adverse pressure gradient of sufficient strength to cause separation. This is point S in Fig. 1. The separation leads to the formation of the shear layer over the bubble and the characteristic flow reversal near the surface. At point T, the shear layer makes a transition to turbulent flow. The static pressure in the bubble is seen to be fairly constant over the bubble until transition. After transition, the magnitude of the reverse flow increases and a vortex type flow is seen in the bubble. Before transition, the reverse flow is very slow, and this area is sometimes referred to as a dead-air region. As the turbulent shear layer entrains high energy external flow, pressure recovery becomes possible, and the bubble reattaches at point R.

Bubbles are usually classified as short or long, not for their length, but for their effect on the flowfield as described by Tani.[2] Short bubbles have only a small, local influence on the airfoil pressure distribution and therefore have little effect on the airfoil performance. The short bubble bursts when it can no longer recover the required pressure. This results in the formation of a long separation bubble. A long bubble is characterized by a significant change in the airfoil pressure distribution. The suction peak on the airfoil leading edge is drastically reduced, reducing the amount of pressure recovery required by the boundary layer in the region of the separation bubble. When the long bubble can no longer provide this pressure recovery, the bubble bursts, and the resulting global change in the pressure distribution and flowfield usually leads to airfoil stall.

In this paper, experimental measurements taken in the separation bubble behind a simulated airfoil ice accretion at low Reynolds number are presented. These data were taken, in

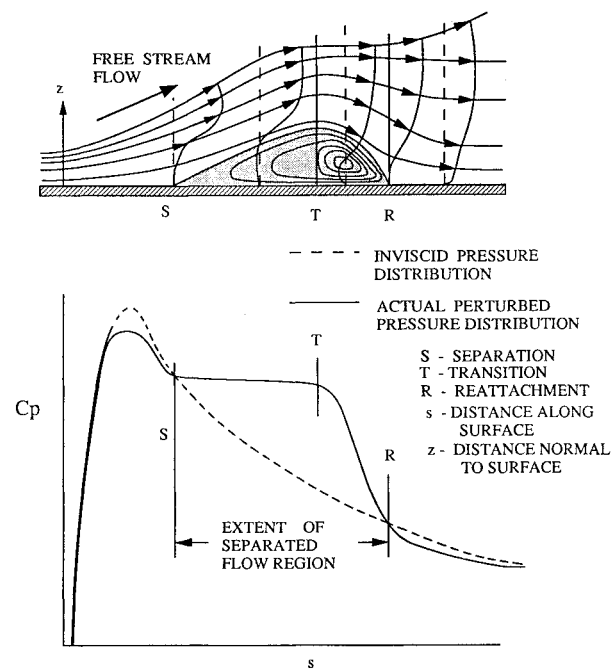


**Fig. 1 Separation bubble, geometry, and pressure.**

Received June 12, 1991; revision received Sept. 20, 1991; accepted for publication Oct. 2, 1991. 

*Associate Professor, Department of Aeronautical and Astronautical Engineering, 101 Transportation Building, 104 S. Mathews Avenue. Associate Fellow AIAA.

†Graduate Research Associate, Department of Aeronautical and Astronautical Engineering, 101 Transportation Building, 104 S. Mathews Avenue. Member AIAA.

‡Project Engineer, 3325 D Triana Boulevard. Member AIAA.

part, to validate the computational methods being developed by Potapczuk[4] and Cebeci[5] for the iced airfoil performance problem. The data consist primarily of surface pressure measurements and time-averaged velocity profiles taken in the bubble with a split hot-film probe.[6-10] The bubble examined here is not the same as the classic laminar separation bubble found on airfoils at low Reynolds number. However, by using the analysis tools developed for those bubbles, many similarities are discovered.

## II. Experimental Procedure

### Apparatus

These tests were conducted in the Ohio State University's (OSU) subsonic wind tunnel located at the Aeronautical and Astronautical Research Laboratory. The tunnel is of conventional design with approximately a 3 × 5 ft test section, 8 ft in length. The tunnel was operated at a speed of 140 ft/s at a Reynolds number based on model chord length of $1.5 \times 10^6$. The tunnel is of open return type and uses four screens and honeycomb in the settling chamber to reduce the tunnel turbulence. Tunnel turbulence intensity as measured with a single hot wire and a 5 kHz low-pass filter is 0.07% at the speeds tested.

A specially built NACA 0012 airfoil model was used for these tests. The model has a 21-in. chord and 39-in. span. A unique feature of this model is its interchangeable leading edges. The simulated ice accretion geometry was obtained by removing the first 15% of the model (about 3 in.) and replacing it with the appropriate airfoil plus ice accretion contour. The ice shape was a simulation of an accretion measured on a 21-in. chord NACA 0012 section tested in the NASA Lewis Icing Research Tunnel. In Fig. 2, the measured and simulated ice profiles are shown. The 5-min profile simulated is a glaze ice shape accreted at 4 deg angle of attack and 130 mph. The icing conditions are a volume median diameter droplet of 20 $\mu$m, liquid water content of 2.1 g/m$^3$, and a temperature of 18°F. Note that the objective here was not to accurately reproduce the measured ice accretion. The objective was to test a representative, but simple, shape to generate data for comparison with ongoing computations. The shape chosen met this objective and could be accurately built and easily and accurately described for input to the numerical methods.

Experience with earlier simulated ice accretion models demonstrated the need for a very dense placement of surface pressure taps. The current model was internally tapped with approximately 90 surface pressure ports. The upper surface was instrumented with a tap every 1% (0.21 in.) of surface length back to the 40% chord station. Another 40 taps were located around the rest of the airfoil, on the model centerline. Pressure measurements were made using a Scanivalve system. The Scanivalves were connected in series sharing one pressure transducer to reduce calibration time and improve the accuracy of the measurements.

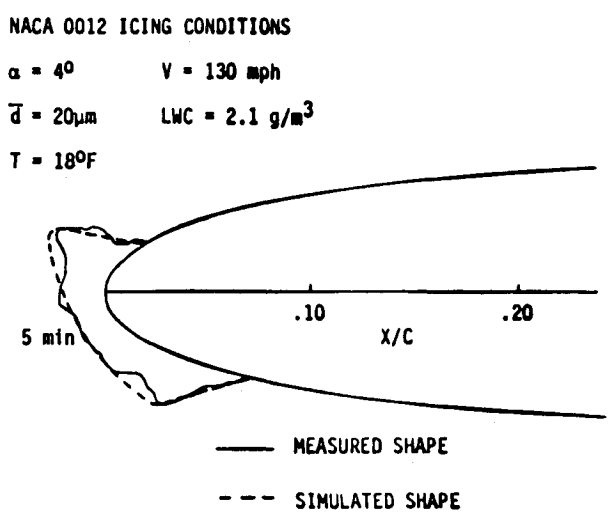


Fig. 2 Measured and simulated ice shape.

To measure the velocity profiles in the separation bubble, a probe capable of determining flow reversal must be accurately positioned in the model boundary layer. A split-film probe, TSI model 1288, was chosen and was used in crossflow. The TSI probe uses two separate films, placed front and back, on the same 0.006-in.-diam fiber rod. The plane of the split is parallel to the axis of the probe, perpendicular to the free-stream flow, thus allowing for the determination of flow reversal. Using a specially designed gauge, the probe was set a known distance, usually 0.025 in., off the surface of the model to start each run. The hot-film data were taken digitally using a TSI IFA100 anemometer and a Harris H800 computer system.

A two-dimensional traversing system was used to position the probe in a horizontal plane on the tunnel centerline. The hot-film probe was supported through an airfoil-shaped strut extending into the tunnel. This steel strut was mounted rigidly to the fixed end of the traverse and moved chordwise (along the tunnel axis) through a sealed slide in the tunnel wall. Probe position was determined using standard potentiometers. Using this system, probe positioning tolerance, including all errors through digitizing, was no more that ± 0.003 in. or ± 0.00014 chord length out from the model and no more than ± 0.010 in. or ± 0.00048 chord length in the chordwise direction.

Flow visualization studies were conducted on the model with the simulated glaze ice accretion. Surface tufts and oil-flow techniques were used as well as oil flow on a model-mounted splitter plate. These techniques are well known and described in Ref. 10. Only the surface oil-flow data will be discussed in this paper.

### Data Reduction

The split-film probe was calibrated in the OSU calibration tunnel. This 4-in.-diam ejector-driven tunnel operates from 0 to 400 ft/s. The probe flow angle can be varied ± 120 deg. The total velocity sensed by the probe was determined from

$$V = f[(E_1 + E_2)^2]$$

where $E_1$ and $E_2$ are the voltages from the front and back of the film, respectively, corrected for ambient temperature effects. The function $f$ is a fourth-order polynomial. The streamwise velocity component $u$ and the perpendicular component $v$ can be determined knowing the flow angle $\phi$. The probe is in end flow when $\phi$ is 0 deg and in crossflow when $\phi$ is 90 deg. Using the expression for sin $\phi$ given in Ref. 11,

$$\sin\phi = \frac{E_1^2 - k^2E_2^2}{(E_1^2 - k^2E_2^2)_{\max}}$$

The constant $k$ is the ratio $E_1/E_2$ at $\phi = 0$ deg and is a function of velocity. The denominator is the value of $E_1^2 - k^2E_2^2$ at $\phi = \pm 90$ deg, depending on the sign of the numerator. This was curve fit based on the calibration data as a polynomial in $V$. Then $u$ and $v$ are

$$v = V \sin\phi, \qquad u = \sqrt{V^2 - v^2}$$

with $u$ greater than zero if $E_1^2 - k^2E_2^2$ is greater than zero. Note that with a two element split-film probe the flow angle can at best be determined only in the range $-90 \le \phi \le 90$ deg. Therefore, the sign of the $v$ component cannot be determined. For a more detailed description of split hot-film calibration and reduction see Spring.[9]

Most of the split film data in this report were taken at 2 kHz over a 1-s interval using a 1 kHz low-pass filter. The $u$ velocity component was calculated for each of the 2000 data points

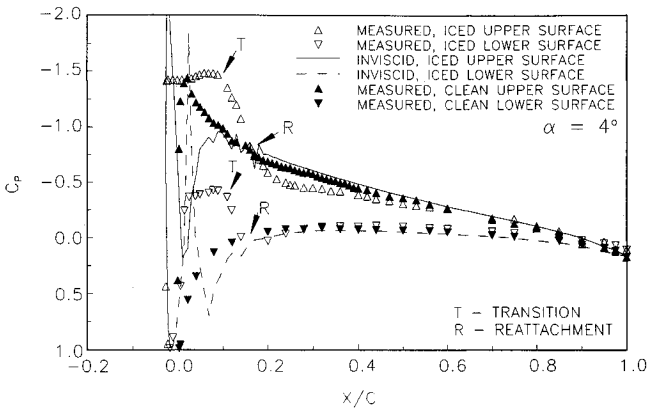


**Fig. 3 Static pressure distribution on a NACA 0012 airfoil with and without simulated ice.**

and averaged to give the mean velocity. This process is repeated at each of the 50 points that make up a single boundary-layer velocity profile. These velocities are the streamwise velocity component $u$; the mean $v$ component and total velocity are unknown by this method.

To calculate the boundary-layer thicknesses $\theta$ and $\delta^*$, an edge velocity must be determined. For these calculations, the edge velocity was assumed to be the maximum velocity measured for that boundary-layer traverse. The displacement thickness was then calculated in the usual way:

$$\delta^*/c = \int_0^{\delta/c} \left(1 - \frac{u}{U_e}\right) \mathrm{d}\left(\frac{y}{c}\right)$$

For profiles that may have reverse flow, the momentum thickness is given by

$$\theta/c = = \int_0^{\delta/c} \left|\frac{u}{U_e}\right| \left(1 - \frac{u}{U_e}\right) \mathrm{d}\left(\frac{y}{c}\right)$$

The stagnation streamline height $y_{stag}$ is merely the height above the surface where the $u$ velocity is zero, separating the reversed flow from the flow in the streamwise direction. The separation streamline $y_{sep}$ is the height above the surface such that all of the fluid below is recirculated in the bubble in a two-dimensional steady model. This is found by integrating up from the surface until the mass of fluid flowing in a reverse sense is equal to that flowing downstream. That is, for constant density flow,

$$\int_0^{y_{sep}/c} \frac{u}{U_e} \mathrm{d}\left(\frac{y}{c}\right) = 0$$

## III. Results and Discussions

This paper primarily deals with the hot-film measurements taken in the separation bubble downstream of the simulated leading-edge ice accretion. However, a brief look at the surface pressures may be useful.

Figure 3 shows the measured surface pressure coefficients for the NACA 0012 airfoil with and without simulated ice, as well as a theoretical prediction[12] of the inviscid flow over the airfoil with simulated ice. The inviscid prediction shows a large negative pressure spike in $C_p$ as the air flows around the ice horns. This occurs at $x/c = -0.0245$ on the upper surface (solid line) and $x/c = 0.0311$ on the lower surface (dashed line). Note that $x/c = 0$ at the uniced airfoil leading edge and $x/c = -0.0266$ at the leading edge of the ice accretion; see Fig. 2. The predicted upper surface $C_p$ spike reaches a value of $-10$. The experimental measurements show that the boundary layer cannot tolerate this severe adverse gradient and separates at these locations on both the upper and lower surfaces. This can easily be seen as the constant pressure regions at $C_p$ values of $-1.4$ on the upper surface and $-0.35$ on the lower. Note that the theory[12] predicts $R_\theta = 150$ in the upper surface laminar boundary layer just ahead of separation, well below that required for transition. Therefore, these are laminar separation bubbles. The large and global change in the pressure distribution from inviscid theory, due to the bubble formation, clearly indicates a long bubble.

The constant pressure region in the upper surface bubble extends to $x/c = 0.08$, labeled T in Fig. 3, where pressure recovery begins. This corresponds to the point of transition in the shear layer.[2] Reattachment occurs downstream of this

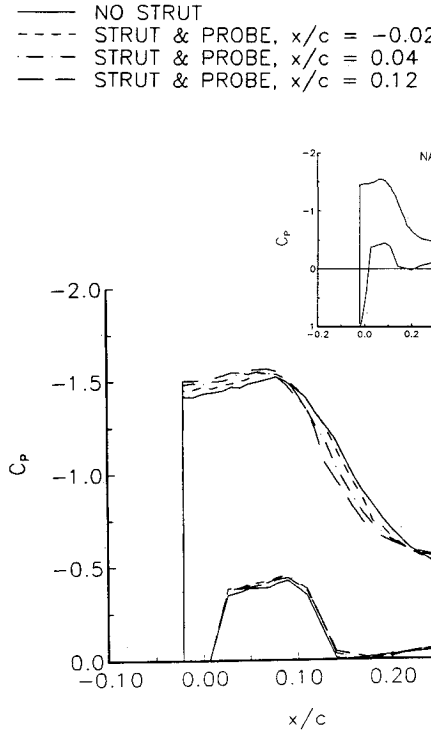


**Fig. 4 Static pressure distributions showing the influence of the strut and probe on the separation bubbles.**

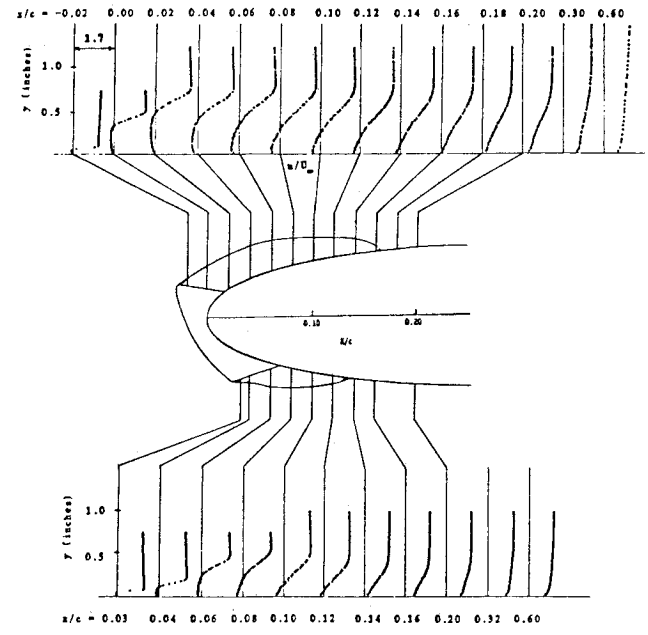


**Fig. 5 Measured velocity profiles on a NACA 0012 airfoil with simulated ice at $\alpha = 4$ deg.**

location, labeled R. For short bubbles, reattachment occurs where the measured pressure recovers to the inviscid, no-bubble, value. For long bubbles, some researchers have found this method of obtaining reattachment no longer valid.[13,14] However, here the $x/c$ location where the measured pressure recovers to the inviscid level, labeled R in Fig. 3, predicts the reattachment point very well. Interestingly, so does the same procedure if the clean airfoil pressures are used in place of the inviscid pressures. Reattachment locations obtained from surface pressures will be compared with flow visualization later in the paper.

It is well known that the presence of a probe can alter the flowfield being measured. This is particularly true for separated flows. To provide some measure of this effect, Fig. 4 presents the measured surface pressures for the iced model with and without the hot-film probe and support system present.[9] Data with the probe at three different locations in the upper surface bubble are shown. These data were taken after an effort was made to reduce the probe support system to the minimum size possible. The influence of the probe and its support is seen as a decrease in the pressure in the constant pressure region over the bubble before transition and an earlier pressure recovery. This indicates a shorter separation bubble. This effect increases as the probe is positioned further back in the bubble. With the probe at $x/c = 0.12$ and using the method of Fig. 3, the pressures indicate a 2% chord reduction in the bubble length. Using a hot-film probe, this type of error is unavoidable.

Hot-film probes in crossflow in a uniform stream see an increased velocity at the film location due to probe support interference. This induced flow may be as large as 16% of the freestream velocity.[9] Here the probe is operated in a shear

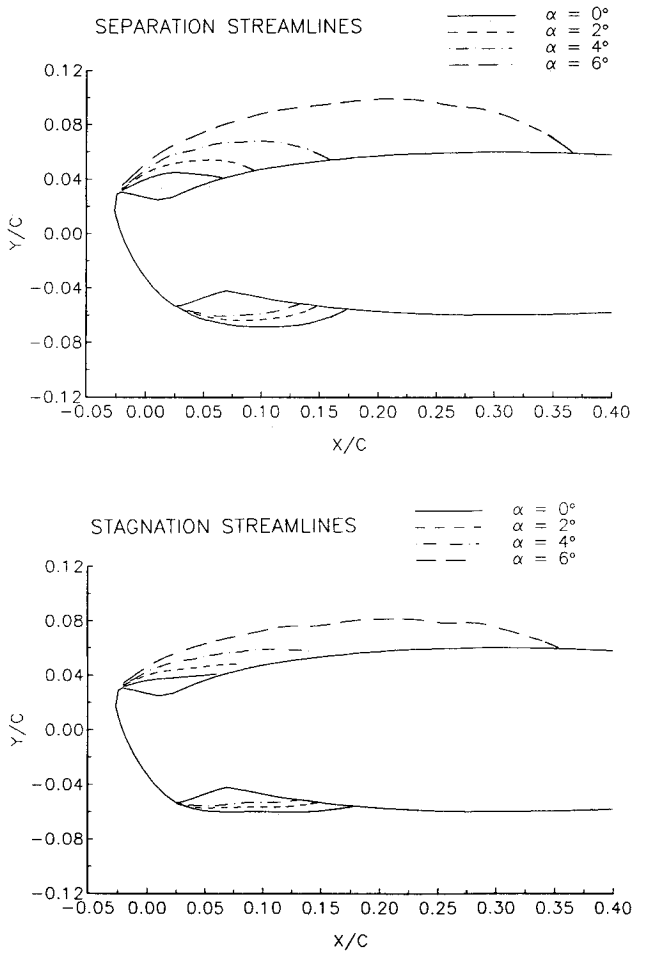


**Fig. 6 Stagnation and separation streamlines from the split-film measurements.**

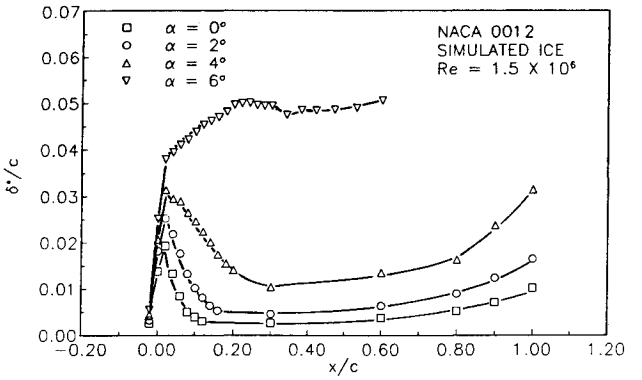


**Fig. 7 Boundary-layer displacement thickness from the split-film measurements.**

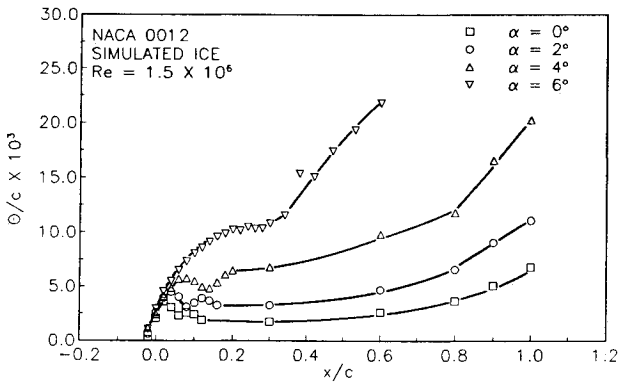


**Fig. 8 Boundary-layer momentum thickness from the split-film measurements.**

flow, and some segments of the supports may be exposed to a different velocity than that at the film sensor. In this case the interference correction is made incorrectly. This will be more severe when the probe is in a very thin shear layer, as at the leading edge of the separation bubble. This results in probe measurements of the magnitude of the reversed flow, for example, to be slightly low. This error should be no more than a few percent of the freestream velocity. These data have not been corrected for this effect due to the lack of an acceptable method.

Figure 5 shows the measured velocity profiles in the upper and lower surface separation bubbles at an angle of attack of 4 deg. A sketch of the model and separation streamline is also shown for reference. First consider the upper surface measurements. The first profile is taken at $x/c = -0.02$, just behind the ice horn. The flow is separated here with a very thin region of reverse and shear flow. The reverse flow region grows rapidly as we move downstream to $x/c = 0.02$. Note that initially the reverse flow in the bubble is very slow. At approximately $x/c = 0.08$, the transition point, the magnitude of the reverse flow has increased and moved nearer the surface. This agrees with the model in Fig. 1 and the theory of Briley and McDonald.[15] As the flow moves further downstream, the shear layer thickens and the amount of reverse flow decreases until the boundary layer reattaches around $x/c = 0.16$. Immediately downstream a distorted turbulent boundary layer is seen. Flow in the lower surface bubble is similar with reattachment of the bubble occurring between $x/c = 0.12$ and 0.14. Similar trends are also seen at 0 and 2 deg angle of attack.

Figure 6 shows the bubble size and shape as indicated by the separation streamlines and the stagnation streamlines at four different angles of attack. At $\alpha = 0$ deg, both upper and lower surface bubbles are quite large. As the angle of attack increases, the upper surface bubble grows slowly from 0 to 2 deg and more rapidly from 2 to 4 deg and 4 to 6 deg. The lower

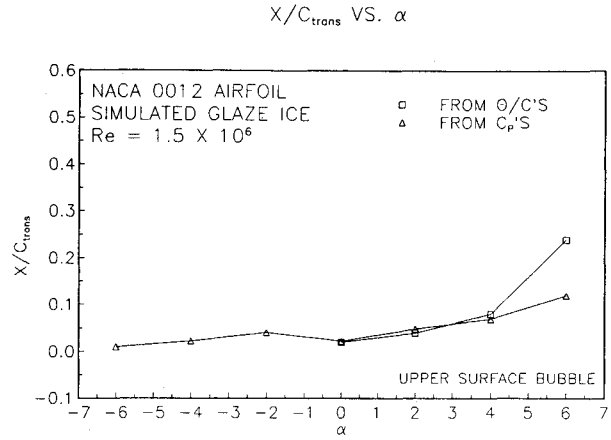


**Fig. 9 Estimated upper surface bubble transition locations.**

surface bubble decreases rapidly in size at first as $\alpha$ is increased but changes little in length between 2 and 4 deg angle of attack. The location of maximum bubble thickness measured normal to the surface occurs at the transition location for bubbles on smooth airfoils.[2,15] However, here due to the surface geometry, this does not correlate to the transition locations indicated by the surface pressures.

Measured values of boundary-layer displacement thickness and momentum thickness obtained from integrating the velocity profiles are shown in Figs. 7 and 8, respectively. Here data are shown at angles of attack of 0, 2, 4, and 6 deg for the upper surface bubble only. Where available, data are shown in the attached turbulent boundary layer downstream of the bubble to the trailing edge.

The displacement thickness is seen initially to grow almost linearly. In all cases, $\alpha = 0$–6 deg, the linear growth is from $x/c = -0.02$ to 0.02. The slope increases as the angle of attack increases. For angles of attack of 0, 2, and 4 deg, a maximum value is reached at $x/c = 0.02$. From the numerical calculations of Crimi and Reeves[16] and Briley and McDonald,[15] $\delta^*$ reaches its maximum value at the transition point. This is the same location where the constant pressure in the bubble ends and pressure recovery begins. The location of $\delta^*_{max}$ seen here does not agree with the transition location. The difference is probably due to the ice shape geometry, Fig. 2. Note that $\delta^*$ reaches a maximum value at $x/c = 0.02$ where the ice shape meets the airfoil contour and the height of the surface above the chord line is a local minima. The $\delta^*$ appears to reflect this special geometry and not the usual trends seen in bubbles on smooth airfoils. However, the plot does show a clear difference in the $\delta^*$ development between the 4- and 6-deg bubbles.

The pressure distributions and lift data of Bragg and Corrier[6] on this geometry show that the bubble begins to grow rapidly between 4 and 6 deg. Maximum lift is at $\alpha = 7$ deg where the upper surface bubble is clearly burst. Khodadoust[10] reports the bubble at $\alpha = 6$ deg and above to be extremely unsteady. It is likely that the bubble at $\alpha = 6$ deg is unsteady and is burst some percentage of the time, changing the character of these time-averaged measurements.

The integrated momentum thickness values are seen in Fig. 8. Initially, as in the $\delta^*$ plots, the growth in $\theta$ is almost linear. For $\alpha = 0$, 2, and 4 deg, this linear region is followed by a local maximum value that increases, and its location moves downstream, as the angle of attack increases. No clear local maximum is seen in the $\alpha = 6$ deg data. Interestingly, the location of the local maxima at $\alpha = 0$, 2, and 4 deg corresponds to the shear layer transition location as indicated by the measured surface pressures. Figure 9 shows the $x/c$ location of the end of the pressure plateau and the location of the local maxima in $\theta/c$. These compare very well at $\alpha = 0$, 2 and 4 deg angle of attack but not at $\alpha = 6$ deg where the character of the bubble has changed.

It is difficult to compare these data with other experiments since most have used hot-wire probes. Since a single hot wire cannot resolve flow direction, reliable mean velocity profiles are not available from which to get $\theta$ and $\delta^*$. However, Briley and McDonald[15] show calculated $\theta/c$ in a laminar separation bubble on a NACA $66_3$-018 airfoil. Their data do not show the initial rapid rise in $\theta/c$ due to their very different geometry. However, a slight reduction in $\theta/c$ is seen in their results after transition with a rapid rise occurring just before reattachment. Therefore, the trend in these data near transition is qualitatively similar to Briley and McDonald, and the $x/c$ locations compare well with the pressure data.

After transition, the $\theta/c$ data decrease with $x/c$, then increase again. At $\alpha = 0$ and 2 deg, a second local maxima is seen, whereas at 4 deg it is not. These $x/c$ values are of 0.08, 0.12, and 0.20, respectively. This rapid rise in $\theta/c$, before the second local maxima, if present, corresponds to trends in Briley and McDonald's $\theta/c$ calculations. The location where $\theta/c$ reaches the second local maxima, or levels off as in the 4-deg case, should compare with the measured reattachment points.

Figure 10 shows the measured reattachment points for both the upper and lower surface separation bubbles. The most accurate and complete measurements of reattachment are those of Khodadoust[10] using surface oil flow. Estimates of the bubble reattachment from surface pressures, the hot-film velocity profiles, and $\theta/c$ values from the hot-film measurements are also shown. The pressure data compare well with the oil flow. Even though this is definitely a long bubble, the simple scheme of determining reattachment by comparing the inviscid and measured pressures, Fig. 3, works quite well. Reattachment from the measured velocity profiles gives bubble reattachment slightly ahead of that from the oil flow. This is to be expected from the probe interference shown in Fig. 4. The prediction of the reattachment point from the $\theta/c$ values compares very well and is downstream of that taken from the velocity profiles directly. This probably indicates a slight error in our analysis of the $\theta/c$ data since it comes from the velocity data and should give the same reattachment location.

The objective of this research was to obtain mean velocity profiles in the separation bubble. Therefore, no detailed study of the unsteady nature of the bubble or shear layer was made. Pfeil and Orth[17] studied shear layer transition and its sensitivity to freestream turbulence on a cylinder with laminar separation bubbles. They found considerable energy at a frequency of 3700 Hz in the shear layer. This corresponded to Tollmien-Schlichting waves in a frequency range where theory has shown that similar Falkner-Skan velocity profiles are unstable. This is well above our sampling rate for the split film. However, a hot wire was used to investigate a low-frequency oscillation seen in the numerical calculations.[4]

Figure 11 shows the power spectrum from a hot-wire probe in the shear layer of the upper surface bubble at $\alpha = 4$ deg. The output shows a clear peak at 11.6 Hz. If this is converted

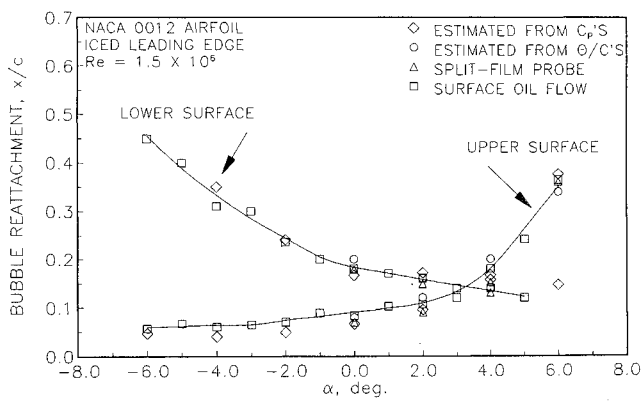


**Fig. 10 Upper surface bubble reattachment location estimated from several different techniques.**

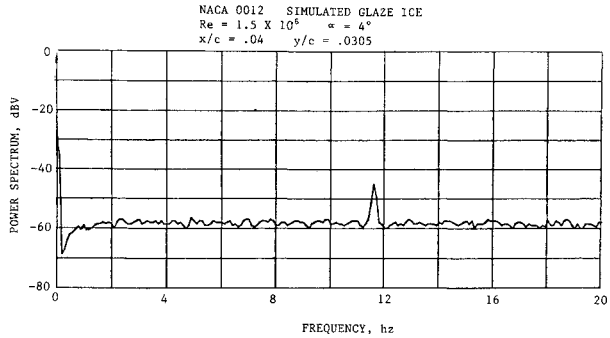


**Fig. 11 Power spectrum of the upper surface bubble shear layer at $\alpha = 4$ deg.**

to a Strouhal number, $S_t = f \cdot h_{ref}/U_\infty$, a value of 0.0185 is found. Here $h_{ref}$ is the airfoil projected height at $\alpha = 4$ deg. For bluff body shedding, a value of $S_t = 0.20$ is usually found. The 0.0185 value corresponds to the low-frequency oscillations found on clean airfoils before stall by Zaman et al.[18] Zaman et al. have found a Strouhal number of approximately 0.02 for many different airfoils. Their work shows that these phenomena occur only for airfoils with "trailing-edge" or "thin-airfoil" type stalls but not for abrupt "leading-edge" stalls involving hysteresis. The separating boundary layer must be in a transitional state. At $\alpha = 4$ deg the airfoil plus ice shape satisfies these conditions. The model is just below its $\alpha = 7$ deg stall angle, it experiences a thin-airfoil stall, and the separating shear layer is transitional.

More recent work by Zaman and Potapczuk[19] has further explored these phenomena as they apply to an airfoil with simulated ice. Although Zaman and Potapczuk's experiment was at a Reynolds number of only $0.1 \times 10^6$, the low-frequency oscillation peaks at between 6 and 7 deg angle of attack. It is interesting that this occurs around the $\alpha = 6$ deg value where the mean flow measurements in the bubble no longer follow the trends seen at lower angles. This reinforces the idea that the 6-deg measurements may be affected by large bubble oscillations.

## IV. Summary

An iced airfoil at low Reynolds number with a simulated leading-edge glaze ice accretion has been studied experimentally. The laminar boundary layer separates due to the severe adverse pressure gradients caused by the simulated ice and forms laminar separation bubbles on both the upper and lower surface. Bubble lengths exceeding 35% chord have been measured.

These bubbles behave in a way remarkably similar to that of more conventional laminar separation bubbles examined by many other researchers. The ice-induced bubbles are classified as long bubbles since a global effect on the airfoil flowfield or pressure distribution is seen. The bubble forms to eliminate the large pressure spike generated by the ice shape and to reduce the pressure recovery required in the bubble. A relatively constant pressure plateau is seen initially over the bubble, followed, as it moves downstream, by a pressure recovery region, then reattachment. The end of the pressure plateau indicates shear layer transition. The $x/c$ location after transition where the measured pressure recovers to the theoretical, inviscid pressure compares well with the reattachment point as measured from flow visualization.

Split-film measured, time-averaged velocities in the bubble show a large region of low velocity reverse flow initially in the bubble. Around transition, and just downstream, a smaller region of higher velocity reverse flow is seen close to the wall. This qualitatively compares well with laminar separation bubble models. Momentum thickness obtained from integrating the measured velocities shows trends that can be used to estimate the $x/c$ location of shear layer transition and bubble reattachment. The $\alpha = 6$ deg data do not follow these trends well, and it is speculated that, for this case, 1 deg below static stall, the bubble is unsteady and bursts some fraction of the time.

Limited time-dependent measurements of the flowfield have identified a low-frequency, 11.6 Hz, oscillation. This corresponds to a Strouhal number of 0.0185 and agrees with recent measurements by other researchers. Strouhal numbers of approximately 0.02 have been observed for flows on similar, and also quite different, geometries.

## Acknowledgments

This work was supported in part by NASA Grant NAG 3-28 while the authors were at the Ohio State University and NAG 3-1134 at the University of Illinois at Urbana-Champaign. The authors acknowledge M. G. Potapczuk of NASA Lewis for his contributions to this research.

## References

[1]Bragg, M. B., "Rime Ice Accretion and Its Effect on Airfoil Performance," Ph.D. Dissertation, Ohio State Univ., Columbus, OH, 1981; also NASA CR 165599, March 1982.

[2]Tani, I., "Low Speed Flows Involving Bubble Separations," *Progress in Aeronautical Science,* Pergamon, New York, 1964, pp. 70–103.

[3]Roberts, W. B., "Calculation of Laminar Separation Bubbles and Their Effect on Airfoil Performance," *AIAA Journal,* Vol. 18, No. 1, 1980, pp. 25–31.

[4]Potapczuk, M. G., "Navier-Stokes Computations for a NACA 0012 Airfoil with Leading Edge Ice," AIAA Paper 87-0101, Jan. 1987.

[5]Cebeci, T., "Effects of Environmentally Imposed Roughness on Airfoil Performance," NASA CR-179639, June 1987.

[6]Bragg, M. B., and Coirier, W. J., "Aerodynamic Measurements of an Airfoil with Simulated Glaze Ice," AIAA Paper 86-0484, Jan. 1986.

[7]Bragg, M. B., and Spring, S. A., "An Experimental Study of the Flow Field about an Airfoil with Glaze Ice," AIAA Paper 87-0100, Jan. 1987.

[8]Bragg, M. B., and Khodadoust, A., "Experimental Measurements in a Large Separation Bubble Due to a Simulated Glaze Ice Accretion," AIAA Paper 88-0116, Jan. 1988.

[9]Spring, S. A., "An Experimental Mapping of the Flow Field Behind a Glaze Ice Shape on a NACA 0012 Airfoil," M.S. Thesis, Ohio State Univ., Columbus, OH, June 1987; also NASA CR 180847, Jan. 1988.

[10]Khodadoust, A., "A Flow Visualization Study of the Leading Edge Separation Bubble on a NACA 0012 Airfoil with Simulated Glaze Ice," M.S. Thesis, Ohio State Univ., Columbus, OH, June 1987; also NASA CR 180846, Jan. 1988.

[11]Boerner, T., and Leutheusser, H. J., "Calibration of Split Fibre Probe for Use in Bubbly Two-Phase Flow," *DISA Information,* No. 29, Jan. 1984, pp. 10–13.

[12]Eppler, R., and Sommers, D. M., "A Computer Program for the Design and Analysis of Low-Speed Airfoils," NASA TM 80210, Aug. 1980.

[13]Arena, A. V., and Mueller, T. J., "Laminar Separation, Transition, and Turbulent Reattachment Near the Leading Edge of Airfoils," *AIAA Journal,* Vol. 18, No. 7, 1980, pp. 747–853.

[14]Horton, H. P., "Laminar Separation Bubbles in Two- and Three-Dimensional Incompressible Flow," Ph.D. Thesis, Univ. of London, Queen Mary College, London, 1968.

[15]Briley, W. R., and McDonald, H., "Numerical Prediction of Incompressible Separation Bubbles," *Journal of Fluid Mechanics,* Vol. 69, Pt. 4, June 1975, pp. 631–656.

[16]Crimi, P., and Reeves, B. L., "Analysis of Leading-Edge Separation Bubbles on Airfoils," *AIAA Journal,* Vol. 14, No. 11, 1976, pp. 1548–1555.

[17]Pfeil, H., and Orth, H., "Boundary-Layer Transition on a Cylinder With and Without Separation Bubbles," *Experiments in Fluids,* Vol. 10, Springer-Verlag, New York, 1990, pp. 23–32.

[18]Zaman, K. B. M. Q., McKinzie, D. J., and Rumsey, C. L., "A Natural Low Frequency Oscillation of the Flow Over an Airfoil Near Stalling Conditions," *Journal of Fluid Mechanics,* Vol. 202, May 1989, pp. 403–442.

[19]Zaman, K. B. M. Q., and Potapczuk, M. G., "The Low Frequency Oscillation in the Flow Over a NACA 0012 Airfoil with an 'Iced' Leading Edge," *Low Reynolds Number Aerodynamics,* edited by T. J. Mueller, Springer-Verlag, New York, 1989, pp. 271–282.